Structural changes in the compounds $LiM_2^{IV}(PO_4)_3$ (M^{IV}=Ge, Ti, Sn, and Hf) as followed by ^{31}P and ^{7}Li NMR

Miguel A. París and Jesús Sanz
Instituto de Ciencia de Materiales de Madrid, Consejo Superior de Investigaciones Científicas (CSIC), 28049 Cantoblanco, Madrid, Spain
(Received 3 December 1996)

From the ^{31}P and ^{7}Li NMR study of the compounds $LiM_2(PO_4)_3$ (M^{IV}=Ge, Ti, Sn, and Hf), structural distortions of the NASICON (acronym for Na superionic conductors) network and the occupation of structural sites by lithium have been analyzed. In compounds with larger cations (M^{IV}=Sn and Hf), structural distortions reduce the ideal symmetry of the NASICON framework (rhombohedral $R\bar{3}c$), producing the differentiation of three phosphorous sites. In these low-symmetry phases, PO_4 tetrahedra distortions, deduced from the analysis of the ^{31}P NMR chemical shift tensor, are higher than those of rhombohedral phases. These additional distortions are eliminated by sample heating above their corresponding transition temperature. On the other hand, from analysis of the dipole and quadrupole interactions of ^{7}Li NMR spectra, recorded at low temperatures, it has been deduced that lithium atoms are located at M_1 sites in the rhombohedral $LiGe_2(PO_4)_3$ and $LiTi_2(PO_4)_3$ and at M_2 sites in the low-symmetry phases of $LiSn_2(PO_4)_3$ and $LiHf_2(PO_4)_3$ compounds. [S0163-1829(97)02821-X]

I. INTRODUCTION

Lithium ion conducting solids is a topic of growing interest because of their potential application as electrolytes in lithium batteries. In particular, lithium compounds with NASICON (acronym for Na superionic conductors) structure and formula $LiM_2(PO_4)_3$ M^{IV}=Ge, Ti, Sn, and Hf, have been extensively studied for their good ionic conductivity.[1–14] The ideal framework of NASICON-type materials,[15–17] shown in Fig. 1(a), is built up by $M_2(PO_4)_3$ units. A pair of MO_6 octahedra are arranged with opposed triangular faces approximately parallel to each other and oriented perpendicularly to the c axis of the structure. The corners of this pair of faces are bridged by three PO_4 tetrahedra, which have one edge approximately parallel to the c axis and the opposed one normal to this axis. Oxygens involved in the second edge form part of octahedra of two adjacent $M_2(PO_4)_3$ units. NASICON compounds have generally a rhombohedral lattice and belong to the space group $R\bar{3}c$, as is the case of M=Ge, Ti; however, some of them as M=Zr, Sn, and Hf, exhibit structural distortions that reduce ideal symmetry.[12,18–21] These distortions can be eliminated by heating the sample above the corresponding phase transition temperature in each of these compounds.

In $LiM_2(PO_4)_3$ compounds, lithium ions can occupy two different sites: (i) M_1 sites, surrounded by six oxygens and located at an inversion center and (ii) M_2 sites, with an irregular tenfold oxygen coordination and disposed symmetrically around the threefold axis of the structure. Both sites alternate along the conduction channels, that form a three-dimensional network [Fig. 1(b)]. At present, little information has been obtained from x-ray diffraction (XRD) data concerning occupation of these sites by lithium in this compounds because of the mobility and the low scattering power of lithium ions. On the other hand, neutron diffraction studies of $LiGe_2(PO_4)_3$ and $Li_{1+x}Ti_{2-x}In_x(PO_4)_3$ (x=0.12) (Refs. 22 and 23) support the preferential occupation of M_1 sites by lithium in these rhombohedral phases; however, there are no results concerning structural sites occupied by lithium in the low-symmetry $LiSn_2(PO_4)_3$ and $LiHf_2(PO_4)_3$ phases.

NMR is a useful tool to investigate distortions in polyhedra and structural positions occupied by atoms. In this work, a systematic ^{31}P NMR study of samples $LiM_2(PO_4)_3$, with M^{IV}=Ti, Ge, Sn, and Hf, has been undertaken to analyze the influence of different tetravalent cations M^{IV} on the structure of these compounds. The ^{7}Li NMR study has been carried out to analyze structural positions occupied by lithium ions.

II. EXPERIMENT

Samples were prepared by calcination at increasing temperatures in the range 850–1600 °C of stoichiometric mixtures of Li_2O, $(NH_4)_2H(PO_4)_3$, and MO_2, where M=Ti, Ge, Sn, and Hf. A more detailed description of the sample preparation is given elsewhere.[9,12,24,25]

^{31}P and ^{7}Li NMR spectra, recorded in static and magic angle spinning (MAS) conditions, were obtained at different temperatures between 25 and −100 °C by using a B-VT 1000/SU07 unit adapted to an MSL 400 Bruker spectrometer. In this study, ^{7}Li spectra were recorded at temperatures for which lithium mobility is absent. For the sake of comparison, data of previously published ^{31}P spectra taken above the phase transition temperature[12,21] are included in this work. The frequency used for ^{31}P and ^{7}Li spectra was 161.96 and 155.5 MHz, respectively. Spectra were taken after $\pi/2$ pulse irradiation. A time interval between successive scans in the range 2–30 s was chosen, depending on the spin-lattice relaxation times of nuclei at the analyzed temperatures. The number of accumulations was in the range 10–200. The ^{7}Li and ^{31}P chemical shifts values are given relative to 1M LiCl and 85% H_3PO_4 aqueous solution, respectively.

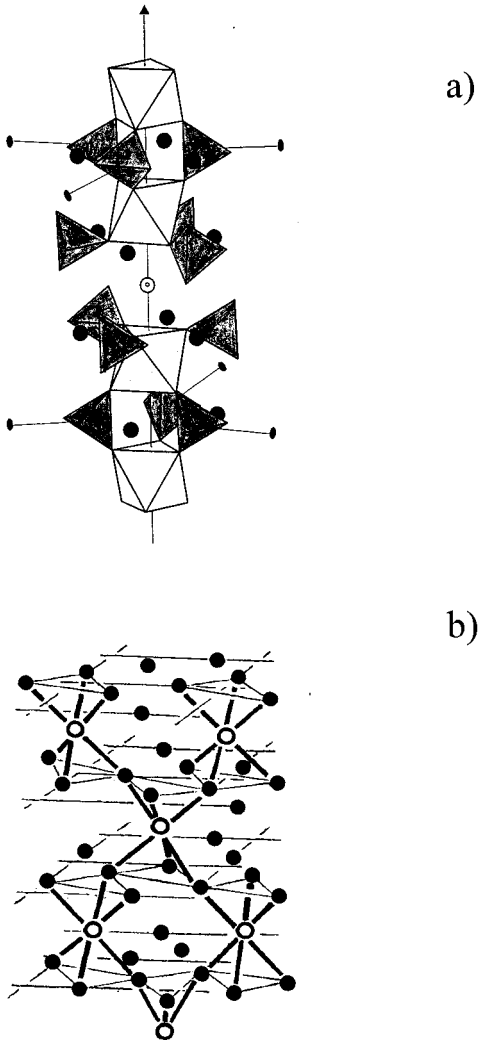

FIG. 1. Schematic representation of (a) NASICON framework; (b) conduction channels connecting both types of structural sites for lithium: M_2 (closed circles) and M_1 (open circles) sites.

The fitting of NMR spectra was carried out with the Bruker WINFIT program,[26] which computes the intensities of the sideband pattern of MAS spectra by the Herzfeld and Berger method.[27] With this program, the position, linewidth, and intensity of components are determined with a standard nonlinear least square method. However, the anisotropies and asymmetry parameters, which characterize nuclear interactions in static and MAS spectra have to be determined by a trial and error procedure.

III. RESULTS

A. ^{31}P NMR

^{31}P ($I=1/2$) static NMR spectra of the low temperature Li$M_2(PO_4)_3$ phases are shown in Fig. 2. A single broad component with asymmetric shape is detected. In order to analyze spectral features, the isotropic shift ($\langle\omega\rangle$) and the second moment ($\Delta\varpi^2$) of static spectra can be calculated through the expressions:

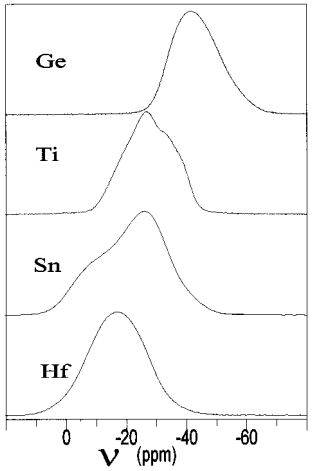

FIG. 2. Static ^{31}P NMR spectra of the Li$M_2(PO_4)_3$ compounds. Spectra were recorded at room temperature, except that of M^{IV} = Hf, which was obtained at $T=250$ K.

$$\langle\omega\rangle=\frac{\int_0^\infty \omega f(\omega)d\omega}{\int_0^\infty f(\omega)d\omega}, \tag{1a}$$

$$\Delta\varpi^2=\frac{\int_0^\infty (\omega-\langle\omega\rangle)^2 f(\omega)d\omega}{\int_0^\infty f(\omega)d\omega}, \tag{1b}$$

where $f(\omega)$ is the experimental shape of the line. It is observed that $\langle\omega\rangle$ changes considerably with composition (Table I). In solids, NMR spectra of nuclei with $I=1/2$ are mainly dominated by dipolar and chemical shift interactions. Nuclear dipolar interactions do not shift positions of NMR lines, therefore, the strong shifts observed in the ^{31}P NMR static spectra indicate that chemical shift interactions are preponderant. On the other hand, the second moment of spectra should be caused by the convolution of the chemical shift anisotropy[28] (CSA) powder pattern and dipolar interactions.

To get information about the chemical shift interactions, the samples were spun in MAS experiments at spinning rates lower than the width of NMR line,[29] expressed in cycles per second. ^{31}P MAS spectra of the compounds are displayed in Fig. 3. A single central line with its corresponding spinning sidebands are observed in the spectra of $LiGe_2(PO_4)_3$ and $LiTi_2(PO_4)_3$ samples; however, MAS spectra of $LiSn_2(PO_4)_3$ and $LiHf_2(PO_4)_3$ exhibit a more complex pattern with three components (insets of Fig. 3). As the chemical environment of all phosphorus atoms is the same, $P(OM^{IV})_4$, the observed components must correspond to the existence of three crystallographic sites in the structure of these compounds. Integration of the sidebands pattern of the three signals gave the same intensities (1:1:1), indicating that the three sites have the same multiplicity. ^{31}P MAS spectra of the last two compounds, heated above their corresponding phase transition temperatures [around 0° in $LiHf_2(PO_4)_3$ and 120 °C in $LiSn_2(PO_4)_3$], display the single component characteristic of rhombohedral phases[12,21] (not shown in Fig. 3).

From analysis of the spinning sidebands pattern of ^{31}P MAS-NMR spectra, the isotropic chemical shift (σ_{iso}), the anisotropy ($\Delta\sigma$), and the asymmetry parameter (η_{cs}) were determined (see Table I). It can be seen that σ_{iso} values are very similar to $\langle\omega\rangle$ values deduced from static NMR pattern,

TABLE I. Isotropic shift ($\langle\omega\rangle$) and second moment ($\Delta\varpi^2$) values were deduced from ^{31}P static NMR spectra. Chemical shift tensor values (σ_{iso}, $\Delta\sigma$, η_{cs}) were deduced from ^{31}P MAS NMR spectra. σ_{11}, σ_{22}, and σ_{33} values were calculated by using Eqs. (2). The letters (R), (M), and (T) stand for rhombohedral, monoclinic, and triclinic phases.

	Static spectra		MAS spectra					
M^{IV}	$\langle\omega\rangle$ [ppm]	$\Delta\varpi^2$ [ppm^2]	σ_{iso} [ppm]	$\Delta\sigma$ [ppm]	η_{cs}	σ_{11} [ppm]	σ_{22} [ppm]	σ_{33} [ppm]
Ge(R)	-43.8 ± 0.1	71 ± 1	-43.6 ± 0.1	-14 ± 0.5	0.65 ± 0.05	-32.1 ± 0.8	-41.1 ± 0.5	-57.6 ± 0.6
Ti(R)	-27.7 ± 0.1	77 ± 1	-27.6 ± 0.1	14 ± 0.5	0.9 ± 0.05	-13.6 ± 0.6[a]	-28.3 ± 0.6	-40.9 ± 0.9
Sn(R)[b]			-23.9 ± 0.1	-11 ± 1	0.8 ± 0.05	-14 ± 0.8	-22.8 ± 0.5	-35 ± 1
Hf(R)[b]			-17.1 ± 0.1	-8 ± 1	1	-9 ± 1	-17.1 ± 0.3	-25 ± 1
			-21.3 ± 0.1	18.0 ± 0.3	0.65 ± 0.05	-3.3 ± 0.4[a]	-24.4 ± 0.6	-36.1 ± 0.8
Sn(M)	-21.9 ± 0.1	130 ± 2	-22.3 ± 0.1	22.3 ± 0.7	0.65 ± 0.05	0.0 ± 0.8[a]	-26.2 ± 0.8	-40 ± 1
			-24.8 ± 0.1	26.3 ± 0.3	0.65 ± 0.5	1.5 ± 0.4[a]	-29.4 ± 0.8	-46 ± 1
			-15.5 ± 0.1	16 ± 1	0.95 ± 0.05	0 ± 1[a]	-15.9 ± 0.4	-31 ± 1
Hf(T)	-17.1 ± 0.1	92 ± 2	-16.5 ± 0.1	18 ± 2	0.95 ± 0.05	1 ± 2[a]	-16.9 ± 0.6	-34 ± 2
			-17.0 ± 0.1	13 ± 3	0.95 ± 0.05	-4 ± 3[a]	-17.3 ± 0.5	-30 ± 3

[a]σ_{33} values were exchanged with σ_{11} ones in order to maintain the structural assignment of axes. See the text for more details.
[b]Chemical shift tensor values were obtained from MAS spectra previously published (Refs. 13 and 21).

both being measures of the chemical shift of ^{31}P NMR lines in these samples. Moreover, the high η_{cs} values obtained in all the phases and the change of $\Delta\sigma$ sign in some of them should be noted. In order to analyze the meaning of $\Delta\sigma$ sign, the principal values of the chemical shift tensor ($\sigma_{11}, \sigma_{22}, \sigma_{33}$) in the principal axes system (PAS) have been calculated. In this reference system, the tensor is diagonal and the principal components are given by[30]

$$\sigma_{11}=\sigma_{iso}-(1+\eta_{cs})\frac{\Delta\sigma}{2}, \tag{2a}$$

$$\sigma_{22}=\sigma_{iso}+(\eta_{cs}-1)\frac{\Delta\sigma}{2}, \tag{2b}$$

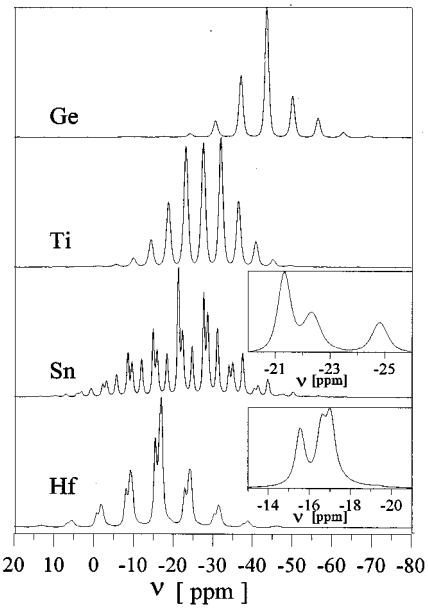

FIG. 3. ^{31}P MAS NMR spectra of the samples obtained at a spinning rate of $\upsilon_r \approx 1000$ Hz. Recording temperatures are the same as those of spectra in Fig. 2. Insets display the central components of ^{31}P MAS spectra of the compounds with M^{IV}=Sn, Hf.

$$\sigma_{33}=\Delta\sigma+\sigma_{iso}. \tag{2c}$$

The principal axes are labeled according to the following convention:

$$|\sigma_{33}-\sigma_{iso}|\geq|\sigma_{11}-\sigma_{iso}|\geq|\sigma_{22}-\sigma_{iso}|. \tag{3}$$

From calculated $\sigma_{11}, \sigma_{22}, \sigma_{33}$ values, it is observed that the change in sign for $\Delta\sigma$ is only due to the change in axis labels induced by the convention expressed in Eq. (3). In order to maintain the structural assignment of principal axes in the discussion that follows below, the criterion (3) has not been respected in the phases with positive $\Delta\sigma$ value, and the values obtained for σ_{11} and σ_{33} have been exchanged in these cases (Table I).

B. ^{7}Li NMR

^{7}Li ($I=3/2$) NMR spectra of the same samples were recorded at temperatures such that lithium mobility is absent. The criterion followed to check the mobility degree was to analyze the temperature dependence of the spin-spin (T_2) and spin-lattice (T_1) relaxation times[28] of the central transition of static spectra. These results are not included in this work and will be published in a separate paper.

In general, the interaction of the quadrupole moment of lithium with the electric field gradient (EFG) at the nuclear site produces a splitting of the satellite transitions ($1/2\rightarrow3/2, -3/2\rightarrow-1/2$) with respect to the central transition ($-1/2\rightarrow1/2$).[28] In powder samples, the broadening of the ^{7}Li central line is generally dominated by dipolar interactions and the pattern of satellite lines is governed by the first-order quadrupole interaction. ^{7}Li NMR static spectra of our compounds are shown in Fig. 4: quadrupole patterns of the compounds with lower symmetry are very different from those of the rhombohedral compounds and cover a wider frequency range. From analysis of these patterns, the quad-

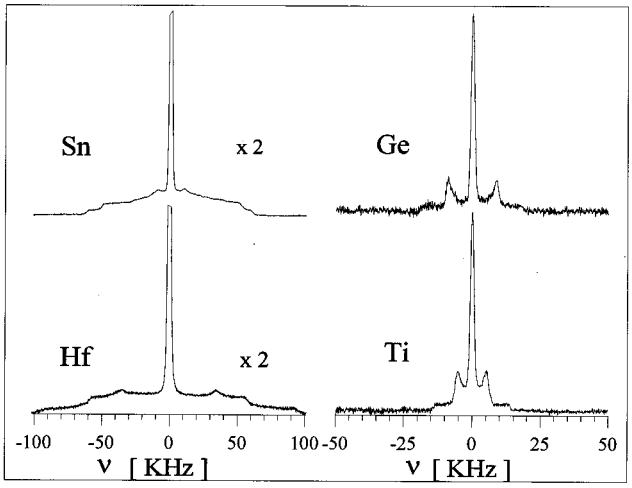

FIG. 4. ^{7}Li static NMR spectra recorded at 270 K for Ge, 167 K for Ti, 273 K for Sn, and 250 K for Hf. It should be noted the different scale in M^{IV}=Sn, Hf spectra with respect to that of the other samples.

rupole coupling constant (C_Q) and the asymmetry parameter (η_Q), has been determined. However, static spectra of samples with high C_Q and η_Q are difficult to record properly and, hence, the analysis of MAS-NMR spectra is more convenient in these cases.

In Fig. 5, ^{7}Li MAS spectra of three representative cases, recorded at the same temperature as the static ones, are shown. Central and satellite transitions are modulated by the spinning sidebands, but the powder pattern of static spectra is clearly reproduced. The MAS spectrum of $LiTi_2(PO_4)_3$ is similar to that of $LiGe_2(PO_4)_3$ and is not included in the figure. C_Q and η_Q values obtained by fitting of MAS spectra coincide with those determined from static spectra and are listed in Table II. It is interesting to remark that C_Q values determined in low symmetry $LiSn_2(PO_4)_3$ and $LiHf_2(PO_4)_3$ phases are considerably higher than those of rhombohedral

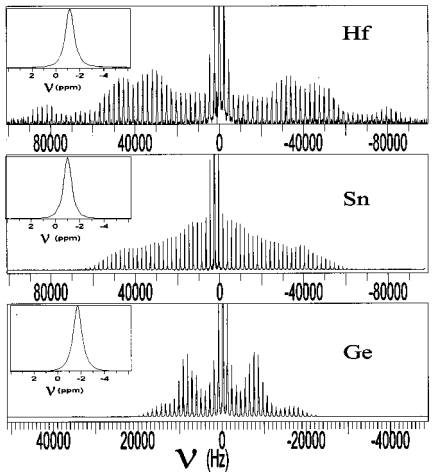

FIG. 5. ^{7}Li MAS NMR spectra of Ge, Sn, and Hf compounds at the same temperatures than those of Fig. 4. Spinning rate ($\upsilon_r \approx 2000$ Hz) and X axis scale of spectra of Sn and Hf members are double than those used for Ge compound. Insets shows the central component at an expanded scale.

TABLE II. Line position of the central component, second moment ($\Delta\varpi^2$), and quadrupole parameters (C_Q and η_Q) deduced from ^{7}Li static and MAS NMR spectra.

M^{IV}	Line position [ppm]	$\Delta\varpi^2$ [G^2]	C_Q [KHz]	η_Q
Ge	-1.7 ± 0.1	0.16 ± 0.02	28 ± 3	0
Ti	-1.4 ± 0.1	0.14 ± 0.01	14 ± 2	0
Sn	-0.7 ± 0.1	0.37 ± 0.03	122 ± 4	0.7 ± 0.05
Hf	-0.7 ± 0.1	0.36 ± 0.03	180 ± 6	0.3 ± 0.03

$LiTi_2(PO_4)_3$ and $LiGe_2(PO_4)_3$ compounds. Moreover, η_Q is zero in the last compounds and have higher values in the first ones.

In the insets of Fig. 5 the central line of ^{7}Li MAS spectra are displayed. In all cases, a single line was observed, whose position changes towards more negative values when going from low-symmetry to rhombohedral compounds (Table II). The position of these lines is mainly given by the isotropic chemical shift, although some influence of second-order quadrupole interaction could be present. The shift associated with this effect has been estimated through the expression[31]

$$\nu^{(2)}_{Q_{(1/2)}} = -\frac{1}{10}\frac{\nu_Q^2}{\nu_0}\left(1+\frac{\eta_Q^2}{3}\right), \tag{4}$$

where ν_0 is the Larmor frequency and ν_Q is related to the quadrupole coupling constant C_Q through the relationship $\nu_Q = 3C_Q/2I(2I-1)$. Substituting obtained C_Q and η_Q values, it can be shown that even in the $LiHf_2(PO_4)_3$, for which the highest value of C_Q has been determined, this effect is practically undetectable ($\nu^{(2)}_{Q_{(1/2)}} = -0.03$ ppm). From these considerations, it is clear that the position of the central line of ^{7}Li MAS spectra is mainly determined by the isotropic chemical shift of nuclei. From this fact, it should be noted that σ_{iso} values of $LiTi_2(PO_4)_3$ and $LiGe_2(PO_4)_3$ are very close each other. The same is true for the low symmetry $LiHf_2(PO_4)_3$ and $LiSn_2(PO_4)_3$ phases, whose values are slightly, but clearly, different from those determined in former samples.

The central transition of NMR static spectra is unaffected by first-order quadrupole interactions but can be broadened by CSA and second-order quadrupole effects. In order to evaluate these contributions, the widths of the central transition were measured at frequencies of 10, 20, and 31 MHz. Values obtained for the linewidths did not change appreciably, indicating that CSA or second-order quadrupole contributions are lower than 100 Hz (the experimental resolution). This agrees with the low CSA values typically reported in ^{7}Li signal (lower than 150 Hz).[32] From these facts, linewidth of the central transition in static ^{7}Li NMR spectra of our compounds is mainly governed by dipolar interactions. A measurement of the linewidth can be obtained from the second moment ($\Delta\varpi^2$), which can be calculated by using the expression (1b). Experimental $\Delta\varpi^2$ values of the low-symmetry $LiHf_2(PO_4)_3$ and $LiHf_2(PO_4)_3$ phases are very close to each other and substantially higher than those obtained in the other two compounds (Table II).

IV. DISCUSSION

It has been reported previously[33] that compounds with general formula $AM_2(PO_4)_3$, where A is an alkali element and M a tetravalent cation (NZP structure), suffer an expansion of the a and c lattice parameters in rhombohedral phases when the M size increases. If the lattice parameters of $LiGe_2(PO_4)_3$ (Ref. 22) and $LiTi_2(PO_4)_3$ (Ref. 23), together with those of the high-temperature phases of $LiSn_2(PO_4)_3$ (Refs. 9, 12, and 20) and $LiHf_2(PO_4)_3$ (Refs. 2 and 13) are considered, this trend is confirmed. This fact seems reasonable as P and M atoms contributes to built up the framework of these compounds.

On the other hand, it was observed in the original NASICON system $[Na_{1+x}Zr_2Si_xP_{3-x}O_{12}\ (0<x<3)]$ (Refs. 16 and 17) that compositions with maximum cell volume $(1.6<x<2.2)$ exhibited structural distortions at room temperature that lowered their symmetry. This observation seems to be confirmed in $LiM_2(PO_4)_3$ compounds, where the presence of three components in ^{31}P MAS spectra (Fig. 3) is only detected in samples with largest tetravalent cations (M=Sn,Hf). This fact is associated with the loss of the threefold and twofold axes of $R3c$ space group, which produces the differentiation of three crystallographic phosphorus sites. In agreement with these observations, XRD patterns of low symmetry $LiSn_2(PO_4)_3$ and $LiHf_2(PO_4)_3$ phases were previously indexed on the basis of monoclinic[12,20] and triclinic[21] lattices, respectively. Heating the samples above the phase transition produces the elimination of the three components and the detection of a single line in ^{31}P MAS NMR spectra. Therefore, structural distortions can be eliminated by increasing the sample temperature, which produces the recovering of the rhombohedral lattice, in the same way as reported for the monoclinically distorted $Na_{1+x}Zr_2Si_xP_{3-x}O_{12}$ $(1.6<x<2.2)$.[34]

In order to analyze the influence of the tetravalent cation on the structure of $LiM_2(PO_4)_3$ compounds, we will discuss first distortions of the structural network and, then, positions occupied by lithium ions in each compound.

A. Influence of the tetravalent cation on the structural distortions

The increase of the size of the tetravalent cations produces variations on the isotropic chemical shift (σ_{iso}) and the anisotropy ($\Delta\sigma$) values of the ^{31}P NMR components. In order to analyze these effects, σ_{iso} and $|\Delta\sigma|$ have been plotted versus the inverse of the effective ionic radius of the tetravalent cation ($1/R$) [Fig. 6(a)]. Radii values have been taken from Shannon and Prewitt's classical reference.[35] As the three lines observed in ^{31}P MAS spectra of low temperature $LiSn_2(PO_4)_3$ and $LiHf_2(PO_4)_3$ phases exhibit very close σ_{iso} and $\Delta\sigma$ values, the average values of these parameters have only been considered. Averaged σ_{iso} values of the low-symmetry $LiSn_2(PO_4)_3$ and $LiHf_2(PO_4)_3$ phases are very close to those observed in rhombohedral phases of the same compounds. From analysis of σ_{iso} values of the different compounds, it is observed that isotropic chemical shift increases very significantly when the size of M^{IV} decreases [Fig. 6(a)]. These findings are reasonable, as $1/R$ represents a measure of the polarizing strength of M^{IV} cations. In general,

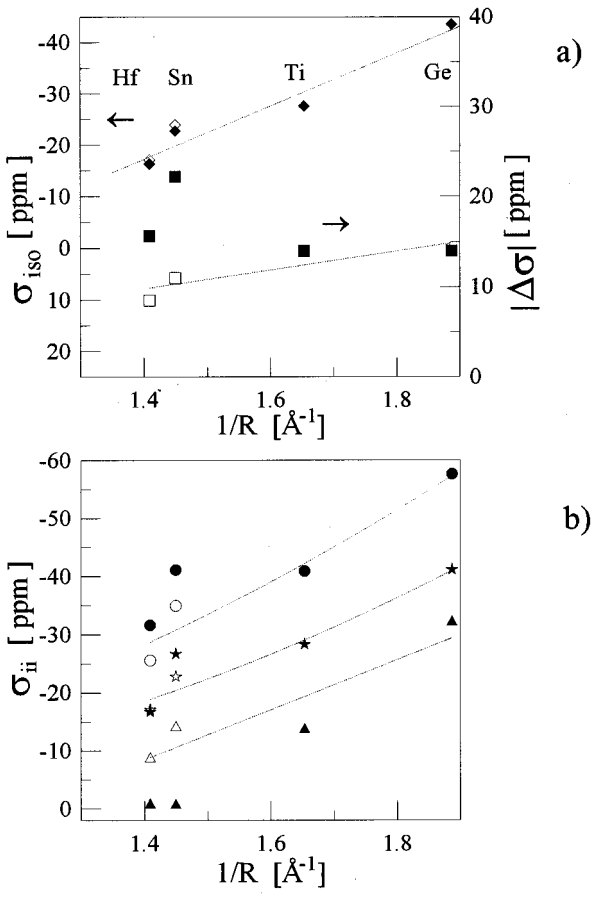

FIG. 6. Plot of (a) the isotropic chemical shift, σ_{iso} (♦); the absolute value of anisotropy, $|\Delta\sigma|$ (■); and (b) the principal values of the chemical shift tensor σ_{11} (▲), σ_{22} (★), σ_{33} (●) versus the inverse of the effective ionic radius of the M^{IV} cation. Open symbols stand for values corresponding to rhombohedral $LiSn_2(PO_4)_3$ and $LiHf_2(PO_4)_3$ phases. Lines are only a guide to show variations in the rhombohedral phases.

cations with larger $1/R$ pulls more effectively the electron density away from oxygen atoms, leaving phosphorus atoms more positively charged. This fact produces a lower antishielding effect on ^{31}P NMR resonance, which explains the more negative σ_{iso} values experimentally observed.

In order to study tetrahedra distortions, η_{cs} and $\Delta\sigma$ values have been analyzed. In all cases, η_{cs} values are important, indicating that the tetrahedra are not perfectly regular. As η_{cs} represents deviation from the axial symmetry in the nucleus neighborhood, deduced values agree with the point symmetry of the tetrahedral site in the rhombohedral (2) or low-symmetry (1) phases. On the other hand, $|\Delta\sigma|$ values, which measure the anisotropy degree of the chemical shift interaction, are in the lower limit of $|\Delta\sigma|$ range obtained for PO_4 tetrahedra in ortophosphates,[36] indicating that tetrahedral distortions are not very important in these compounds. If $|\Delta\sigma|$ value is plotted as a function of $1/R$ [Fig. 6(a)], it is observed that in the rhombohedral phases it changes much less than σ_{iso}; however, it increases considerably in the low symmetry phases with respect to the rhombohedral ones. From these facts, it can be concluded that tetrahedral geometry is not very affected by the size of M^{IV} cation in the rhombohedral phases; however, it changes appreciably in the

TABLE III. Experimental and calculated second moments corresponding to lithium occupying the M_1 and M_2 sites. Experimental values were deduced from the central transition of ^{7}Li NMR static spectra. Relative Li-Li and Li-P contributions ($\Delta\varpi^2_{\text{Li-Li}}$, $\Delta\varpi^2_{\text{Li-P}}$) were calculated with expression (5) of the text. Distances Li-P and Li-Li were calculated by using a rhombohedral lattice in all the cases (see the text).

	M_1 site					M_2 site					
M^{IV}	$r_{\text{Li-P}}$ [Å]	$r_{\text{Li-Li}}$ [Å]	$\Delta\varpi^2_{\text{Li-P}}$ [G^2]	$\Delta\varpi^2_{\text{Li-Li}}$ [G^2]	$\Delta\varpi^2_{\text{cal}}$ [G^2]	$r_{\text{Li-P}}$ [Å]	$r_{\text{Li-Li}}$ [Å]	$\Delta\varpi^2_{\text{Li-P}}$ [G^2]	$\Delta\varpi^2_{\text{Li-Li}}$ [G^2]	$\Delta\varpi^2_{\text{cal}}$ [G^2]	Expt. $\Delta\varpi^2$ [G^2]
Ge	3.42/5.64	5.87	0.10	0.04	0.14	2.49/3.44	5.87	0.36	0.04	0.40	0.16±0.02
Ti	3.49/5.78	6.00	0.09	0.04	0.13	2.58/3.51	6.00	0.29	0.04	0.33	0.14±0.01
Sn	3.57/5.86	6.15	0.08	0.03	0.11	2.60/3.44	6.15	0.29	0.03	0.32	0.37±0.03
Hf	3.64/5.98	6.27	0.07	0.03	0.10	2.66/3.49	6.27	0.27	0.03	0.30	0.36±0.03

low temperature $LiSn_2(PO_4)_3$ and $LiHf_2(PO_4)_3$ phases. These observations agree with results obtained by neutron diffraction in the NASICON compounds $Na_{1+x}Zr_2Si_xP_{3-x}O_{12}$ ($x=1.6,2.0$),[34] which showed less distorted tetrahedra in rhombohedral than in monoclinic phases.

From analysis of σ_{11}, σ_{22}, and σ_{33} values [Fig. 6(b)], it is observed that they increase as the tetravalent cation size decreases in the rhombohedral phases, following the same trend than σ_{iso}. However, it can be seen that while the variation in the σ_{22} direction is not very important in the low-symmetry phases with respect to that found in the rhombohedral phases, the values along the other two directions vary appreciably in opposite senses. These variations could be related to tetrahedral distortions induced by the different rotation of the vertical and horizontal tetrahedral edges around a direction perpendicular to the c axis (coincident with the twofold axis of the $R3c$ symmetry) observed in $Na_{1+x}Zr_2Si_xP_{3-x}O_{12}$ ($x=1.6,2.0$).[34] In these compounds, it was found that rotation of the two edges was similar and lower in the rhombohedral phases than in the monoclinic ones. These observations could explain the higher differentiation of experimental σ_{11} and σ_{33} values as measured in the low symmetry $LiSn_2(PO_4)_3$ and $LiHf_2(PO_4)_3$ phases.

B. Distribution of lithium ions

1. Calculation of second moment ($\Delta\varpi^2$)

The existence of a single line in the low temperature ^{7}Li MAS spectra of all the samples, shown in the insets of Fig. 5, indicates that lithium occupies only one type of site in each compound. If it is remembered that the broadening of the central line of ^{7}Li static spectra in our samples is mainly due to dipolar interactions, the study of linewidth could be used to analyze the environment of lithium in these compounds. To that end, the experimental second moment ($\Delta\varpi^2$) of the central line in ^{7}Li static spectra can be compared with those deduced from the Van Vleck's expression for a rigid lattice in powder samples:[37]

$$\Delta\varpi^2=\frac{3}{5}\,\gamma_I^4\hbar^2 I(I+1)\sum_k \frac{1}{r_{jk}^6}+\frac{4}{15}\,\gamma_1^2\gamma_s^2\hbar^2 S(S+1)\sum_k \frac{1}{r_{jk}^6}. \quad (5)$$

The first term accounts for dipolar interactions between like spins and the second one between unlike spins. γ_I and γ_S are the gyromagnetic ratios for the I and S spins and r_{jk} is the distance between interacting spins.

The most important contributions to the second moment of ^{7}Li NMR line in these compounds are the Li-Li and Li-P dipolar interactions, because of the low magnetic moments of the other elements in these compounds. In order to calculate the interatomic distances Li-Li and Li-P in the rhombohedral phases of $LiGe_2(PO_4)_3$ and $LiTi_2(PO_4)_3$, lattice parameters and relative atomic positions are taken from Refs. 23 and 22 respectively. In the low symmetry phases of $LiSn_2(PO_4)_3$ and $LiHf_2(PO_4)_3$, lattice parameters are available but, unfortunately, atomic coordinates have not been reported yet. Therefore, in order to estimate the interatomic distances in these compounds, the relative atomic coordinates for the rhombohedral $LiTi_2(PO_4)_3$ were used. This procedures assumes that interatomic distances in the low-symmetry phases do not change very much with respect to rhombohedral ones, what it has been confirmed in the $Na_{1+x}Zr_2Si_xP_{2-x}O_{12}$ ($x=1.6,2.0$) compounds.[34]

Second moments estimated for lithium ions occupying the M_1 and M_2 sites, are shown in Table III. In this table, distances between lithium atoms and nearest lithium and phosphorus neighbors are given for each site. It can be seen that Li-P dipolar interaction is much important than Li-Li one, irrespective of the site lithium ions occupy. If the experimental $\Delta\varpi^2$ value of each compound is compared with calculated $\Delta\varpi^2$, a good agreement is obtained for lithium occupying the M_1 sites in $LiGe_2(PO_4)_3$ and $LiTi_2(PO_4)_3$. Deduced occupation of M_1 sites by lithium in rhombohedral phases supports neutron diffraction results previously reported.[22,23] In the case of $LiSn_2(PO_4)_3$ and $LiHf_2(PO_4)_3$, experimental $\Delta\varpi^2$ values are very similar to those calculated for lithium occupying M_2 sites.

The fact that lithium ions occupy the same type of site in the $LiSn_2(PO_4)_3$ and $LiHf_2(PO_4)_3$ is also supported by the very close σ_{iso} values deduced from ^{7}Li MAS spectra of these compounds. These values are slightly but significantly different from those deduced in the rhombohedral $LiGe_2(PO_4)_3$ and $LiTi_2(PO_4)_3$, which are again very close to each other. All these observations suggest that, in absence of mobility, lithium ions occupy different sites in the rhombohedral (M_1 sites) and in the monoclinic/triclinic (M_2 sites) compounds.

2. Calculation of the quadrupole coupling parameters

Another way to analyze structural positions occupied by lithium is the study of the quadrupole coupling parameters, C_Q and η_Q, which can be expressed as[28]

$$C_Q=\frac{e^2QV_{zz}}{h}, \quad \eta_Q=\frac{V_{xx}-V_{yy}}{V_{zz}}, \tag{6}$$

where Q is the quadrupole moment of nuclei and V_{xx}, V_{yy}, V_{zz} are the principal values of the electric field gradient (EFG) tensor at the position of the nuclei. The criterion followed to label the principal axes is

$$|V_{zz}|\geqslant|V_{yy}|\geqslant|V_{xx}|. \tag{7}$$

C_Q measures the deviation of the structural environment of nuclei from cubic symmetry. On the other hand, $\eta_Q=0$ indicates that the environmental has axial symmetry and $\eta_Q>0$ that it has a lower symmetry.

Assuming that the compounds are predominantly ionic, the components of the EFG tensor can be calculated on the basis of a point charge model through the expression

$$V_{ij}=\frac{1}{4\pi\varepsilon_0}\sum_k eZ_k\frac{3x_i^k-r_k^2\delta_{ij}}{r_k^5}, \tag{8}$$

where eZ_k is the electric charge of the kth ion. The principal components of the EFG tensor are obtained by subsequent diagonalisation of matrix V_{ij} and C_Q and η_Q are determined through Eqs. (6). Although η_Q can be calculated directly from the EFG tensor, calculation of C_Q requires an estimate of the Sternheimer shielding factor,[38–40] γ_∞ [$C_Q=e^2Q(1-\gamma_\infty)V_{zz}/h$], which accounts for distortions induced in the core electrons of the ion by the quadrupolar field of the nucleus and by the external field gradients. For Li^+, γ_∞ values lie in the range 0.25–0.34,[41–44] hence in the following calculations γ_∞ value has been taken as 0.3. The summation indicated by Eq. (8) is performed numerically in a Cartesian coordinate system with the Z axis along the c axis of the unit cell and the X and Y axes in the perpendicular plane. It was found that convergence in V_{ij} calculations, with errors less than 2%, could be obtained if all ions within a radius of 30 Å are considered. The EFG tensor can be expressed as a sum of the contributions corresponding to each sublattice:

$$V_{ij}=Z_{\mathrm{Li}}V_{ij}^{\mathrm{Li}}+Z_MV_{ij}^M+Z_{\mathrm{P}}V_{ij}^{\mathrm{P}}+Z_{\mathrm{O}_1}V_{ij}^{\mathrm{O}_1}+Z_{\mathrm{O}_2}V_{ij}^{\mathrm{O}_2}. \tag{9}$$

O_1 and O_2 sublattices are constituted by the oxygens forming the horizontal and vertical edges of PO_4 tetrahedra, respectively.

Rhombohedral phases. In our calculation, the same lattice parameters and atomic coordinates than those used in the previous section have been taken. In this analysis, calculations carried out on the rhombohedral $LiGe_2(PO_4)_3$ and $LiTi_2(PO_4)_3$ will be presented first. By explicit calculation of V_{ij} at M_1 site of $LiGe_2(PO_4)_3$, it is obtained

$$\bar{\bar{V}}=Z_{\mathrm{Li}}\begin{pmatrix}2\times10^{-3}&0&0\\0&2\times10^{-3}&0\\0&0&-5\times10^{-3}\end{pmatrix}+Z_{\mathrm{Ge}}\begin{pmatrix}-0.90&0&0\\0&-0.90&0\\0&0&1.83\end{pmatrix}+Z_{\mathrm{P}}\begin{pmatrix}0.18&2\times10^{-4}&-2\times10^{-4}\\2\times10^{-4}&0.18&2.0\times10^{-4}\\-2\times10^{-4}&2.0\times10^{-4}&0.36\end{pmatrix}$$
$$+Z_{\mathrm{O}_1}\begin{pmatrix}0.26&-2\times10^{-4}&0\\-2\times10^{-4}&0.26&0\\0&0&0.53\end{pmatrix}+Z_{\mathrm{O}_2}\begin{pmatrix}-2.62&3\times10^{-4}&3\times10^{-4}\\3\times10^{-4}&-2.62&-2\times10^{-4}\\3\times10^{-4}&-2\times10^{-4}&5.24\end{pmatrix}\ [\mathrm{V/Å^2}] \tag{10}$$

From simple inspection of this expression, some interesting features can be deduced. The principal contribution to the EFG at M_1 site is due to the O_2 and Ge sublattices and contribution of the other lithium ions is negligible. Moreover, as all matrices are almost diagonal, the resulting EFG tensor is diagonal. Therefore, the c direction of the unit cell is the Z axis of the principal axis system (PAS) associated with the quadrupole interaction in M_1 sites. It is also found that, whichever effective charge of each atom is chosen, η_Q is equal to zero. However the V_{zz} principal component of the EFG tensor depends on the effective charges of the atoms through the expression

$$V_{zz}=(-5\times10^{-3})Z_{\mathrm{Li}}+1.83Z_{\mathrm{Ge}}+0.36Z_{\mathrm{P}}+0.53Z_{\mathrm{O}_1}+5.24Z_{\mathrm{O}_2}\ [\mathrm{V/Å^2}]. \tag{11}$$

If the EFG tensor at M_1 sites of $LiTi_2(PO_4)_3$ is now calculated, similar results are obtained. Experimental η_Q values obtained from ^{7}Li NMR spectra of rhombohedral $LiGe_2(PO_4)_3$ and $LiTi_2(PO_4)_3$ are zero, confirming that lithium ions occupy M_1 sites in these compounds. However, C_Q values calculated by using nominal charges are considerably higher ($C_Q=376$ and 263 KHz, respectively) than those experimentally observed ($C_Q=28$ and 14 KHz). This fact indicates that the structural framework has a partial covalent character and that a net reduction of atoms charge is produced. Therefore, more realistic effective charges have to be considered in C_Q calculations.

In order to simplify the problem, two assumptions are going to be made: first, a fully ionized lithium is considered ($Z_{\mathrm{Li}}=+1$) and, second, the effective charges for the two types of oxygen are assumed to be equal ($Z_{\mathrm{O}}=Z_{\mathrm{O}_1}=Z_{\mathrm{O}_2}$). Both suppositions seems to be reasonable and not very restrictive in our analysis. Taking into account these hypotheses and the condition of electrical neutrality, the only free parameters in Eq. (11) are Z_{Ge} and Z_{P}. In the following calculations, it has been admitted the same charge sets for

TABLE IV. Experimental and calculated quadrupole coupling constant (C_Q) and asymmetry parameter (η_Q) values. Calculated C_Q and η_Q values for lithium occupying M_1 and M_2 sites were obtained under hypothesis discussed in the text.

	Experimental		M_1 site		M_2 site	
M^{IV}	C_Q [KHz]	η_Q	C_Q [KHz]	η_Q	C_Q [KHz]	η_Q
Ge	28±3	0	24±3	0	178±17	0.51±0.02
Ti	14±2	0	13±3	0	140±12	0.63±0.02
Sn	122±4	0.7±0.05	37±4	0	126±14	0.51±0.02
Hf	180±6	0.3±0.03	35±5	0	118±12	0.53±0.02

$LiGe_2(PO_4)_3$ and $LiTi_2(PO_4)_3$. We have searched for possible solutions reproducing simultaneously the experimental C_Q values in both samples and have found that the solution is not unique. Excluding meaningless cases, charge sets fulfilling the condition $Z_M = 1.4Z_P + 0.2$, with $2 < Z_P < 2.5$, would reproduce reasonably well the experimental data (see Table IV). If the EFG tensor at the M_2 sites were now calculated on this basis, the C_Q values obtained would be much higher than the experimental ones and η_Q values significantly different from zero (Table IV).

Low-symmetry phases. Experimental C_Q values of low-symmetry $LiSn_2(PO_4)_3$ and $LiHf_2(PO_4)_3$ phases are higher than in the rhombohedral $LiGe_2(PO_4)_3$ and $LiTi_2(PO_4)_3$ phases. Moreover, experimental η_Q values are different from zero, indicating that the lithium environment has no axial symmetry. If the same effective charges as deduced in the analysis of rhombohedral compounds are considered, occupation of M_1 sites by lithium in low-symmetry $LiSn_2(PO_4)_3$ and $LiHf_2(PO_4)_3$ phases must be clearly disregarded (Table IV). On the other hand, if occupation of M_2 sites is considered, an analogous expression to Eq. (10) can be obtained for M_2 sites. For the low symmetry $LiSn_2(PO_4)_3$ phase the EFG tensor can be written as

$$\bar{\bar{V}} = Z_{Li}\begin{pmatrix} 0.20 & 0.11 & 0.03 \\ 0.11 & 0.09 & 0.24 \\ 0.03 & 0.24 & -0.29 \end{pmatrix} + Z_{Sn}\begin{pmatrix} 0.08 & 0.06 & -0.56 \\ 0.06 & 0.15 & 0.32 \\ -0.56 & 0.32 & -0.23 \end{pmatrix} + Z_{P}\begin{pmatrix} 0.67 & -0.33 & -0.15 \\ -0.33 & 0.28 & 0.09 \\ -0.18 & 0.09 & -0.95 \end{pmatrix} + Z_{O_1}\begin{pmatrix} -0.84 & 1.09 & -1.33 \\ 1.09 & 0.43 & 0.77 \\ -1.33 & 0.77 & 0.41 \end{pmatrix} + Z_{O_2}\begin{pmatrix} 2.54 & -2.24 & 0.25 \\ -2.24 & -0.04 & -0.14 \\ 0.25 & -0.14 & -2.50 \end{pmatrix} \quad [V/Å^2]. \tag{12}$$

In this case, $\bar{\bar{V}}$ is not diagonal. From this fact, diagonalization of $\bar{\bar{V}}$ tensor is a previous step in the evaluation of the principal components for each charge set. If values of quadrupole parameters associated to M_2 sites are calculated, by using the same hypothesis as in the previous cases, it is found that the local symmetry at M_2 site is not axial ($\eta_Q \neq 0$) and that the magnitude of the quadrupole interaction (C_Q) is much higher than that at M_1 site. The reasonably good agreement obtained between calculated and experimental values suggests that lithium ions occupy preferentially M_2 sites in the low temperature $LiHf_2(PO_4)_3$ and $LiSn_2(PO_4)_3$ phases, supporting again conclusions obtained from the $\Delta\varpi^2$ analysis. However, a structural refinement of these phases (not available at present) would be interesting to reproduce more accurately experimental C_Q and η_Q values of low temperature $LiHf_2(PO_4)_3$ and $LiSn_2(PO_4)_3$ phases, and to explain the observed differences in both compounds.

V. CONCLUSIONS

From ^{31}P and ^{7}Li NMR study of $LiM_2(PO_4)_3$ (M^{IV} = Ge, Ti, Sn, and Hf), structural distortions of the NASICON network and lithium location over two possible structural sites has been analyzed.

The increase of the tetravalent cation M^{IV} size in the family $LiM_2(PO_4)_3$ (M^{IV} = Ge, Ti, Sn, and Hf) produces an expansion of the unit cell that is responsible for the structural distortions of the NASICON framework, lowering the ideal $R3c$ symmetry in the M^{IV} = Sn and Hf members. These structural distortions produce the differentiation of three nonequivalent crystallographically phosphorus sites, detected in ^{31}P MAS NMR spectra. By heating the low-symmetry phases, the onset of a phase transition produces the recovering of the usual rhombohedral lattice of NASICON compounds.

From analysis of CSA interactions deduced from ^{31}P NMR signal, it has been shown that isotropic chemical shift values depend strongly on the polarizing strength of the tetravalent cation. Moreover, it has been observed that PO_4 tetrahedra distortions are much higher in the low symmetry phases than in the rhombohedral ones. However, the distortions of the tetrahedral geometry in the rhombohedral phases are not much affected by the cation size.

Finally, from analysis of ^{7}Li NMR spectra it has been shown that, in absence of ionic mobility, lithium occupies different structural positions in the analyzed compounds. M_1 sites in the rhombohedral $LiGe_2(PO_4)_3$ and $LiTi_2(PO_4)_3$, and M_2 sites in the low temperature $LiSn_2(PO_4)_3$ (monoclinic) and $LiHf_2(PO_4)_3$ (triclinic) phases.

ACKNOWLEDGMENTS

The authors wish to thank A. Martínez-Juárez for sample preparation and Dr. J. M. Rojo and Dr. J. E. Iglesias for fruitful discussions. This work was supported by the CICYT (Spain) under Project No. MAT95-0899.

[1] R. D. Shannon, B. E. Taylor, A. D. English, and T. Berzins, Electrochem. Acta **22**, 783 (1977).
[2] B. E. Taylor, A. D. English, and T. Berzins, Mater. Res. Bull. **12**, 171 (1977).
[3] M. A. Subramanian, R. Subramanian, and A. Clearfield, Solid State Ion. **18&19**, 562 (1986).
[4] S. Hamdoune, D. Tran Qui, and E. J. L. Schouller. Solid State Ion. **18&19**, 587 (1986).
[5] S. Li, J. Cai, and Z. Lin, Solid State Ion. **28&30**, 1265 (1988).
[6] B. V. R. Chowdari, K. Radhakrishnan, K. A. Thomas, and G. V. Subba Rao, Mater. Res. Bull. **24**, 221 (1989).
[7] H. Aono, E. Sugimoto, Y. Sadaoka, N. Imanaka, and G. Adachi, J. Electrochem. Soc. **137**, 1023 (1990).
[8] H. Aono, E. Sugimoto, Y. Sadaoka, N. Imanaka, and G. Adachi, Solid State Ion. **47**, 257 (1991).
[9] J. Winand, A. Rulmont, and P. Tarte, J. Solid State Chem. **93**, 341 (1991).
[10] H. Aono, E. Sugimoto, Y. Sadaoka, N. Imanaka, and G. Adachi, J. Electrochem. Soc. **140**, 1827 (1993).
[11] J. Kuwano, N. Sato, M. Kato, and K. Takano, Solid State Ion. **70/71**, 332 (1994).
[12] A. Martínez-Juárez, J. M. Rojo, J. E. Iglesias, and J. Sanz, Chem. Mater. **7**, 1857 (1995).
[13] A. Martínez-Juárez, J. E. Iglesias, and J. M. Rojo, Solid State Ion. **91**, 295 (1996).
[14] M. A. París, A. Martínez-Juárez, J. M. Rojo, and J. Sanz, J. Phys. Condens. Matter **8**, 5355 (1996).
[15] L. Hagman and P. Kierkegaard, Acta Chem. Scand. **22**, 1822 (1968).
[16] J. B. Goodenough, H. Y. Hong, and J. A. Kafalas, Mater. Res. Bull. **11**, 203 (1976).
[17] H. Y. Hong, Mater. Res. Bull. **11**, 173 (1976).
[18] D. Petit, Ph. Colomban, G. Collin, and J. P. Boilot, Mater. Res. Bull. **21**, 365 (1986).
[19] F. Sudreau, D. Petit, and J. P. Boilot, J. Solid State Chem. **83**, 78 (1989).
[20] J. Angenault, J. C. Couturier, J. P. Souron, D. Siliqi, and M. Quarton, J. Mater. Sci. Lett. **11**, 1705 (1992).
[21] M. A. París, A. Martínez-Juárez, J. M. Rojo, J. E. Iglesias, and J. Sanz, Chem. Mater. (to be published).
[22] D. Tran Qui, S. Hamdoune, J. L. Soubeyroux, and E. Prince, J. Solid State Chem. **72**, 309 (1988).
[23] M. Alami, R. Brochu, J. L. Soubeyroux, P. Gravereau, G. Le Flem, and P. Hagenmuller, J. Solid State Chem. **90**, 185 (1991).
[24] R. Masse. Bull. Soc. Fr. Mineral. Cristallogr. **93**, 500 (1970).
[25] A. Martínez, J. M. Rojo, J. E. Iglesias, J. Sanz, and R. M. Rojas, Chem. Mater. **6**, 1790 (1994).
[26] D. Massiot, WINFIT programme, ©Bruker-Franzen Analytik GmbH, 1993.
[27] J. Herzfeld and E. Berger. J. Chem. Phys. **73**, 6021 (1980).
[28] A. Abragam, *The Principles of Nuclear Magnetism* (Oxford University Press, Oxford, 1961).
[29] M. M. Maricq and J. S. Waugh, J. Chem. Phys. **70**, 3300 (1979).
[30] V. Haeberlen, Adv. Magn. Reson., Suppl. 1 (1976).
[31] D. Freude, J. Haase, J. Klinowski, T. A. Carpenter, and G. Ronikier, Chem. Phys. Lett. **119**, 365 (1985).
[32] C. Brevar and P. Granger, *Handbook of High Multinuclear NMR* (Wiley, New York, 1981).
[33] J. Alamo and R. Roy, J. Mater. Sci. **21**, 444 (1986).
[34] J.-J. Didisheim, E. Prince, and J. Wuensch, Solid State Ion. **18&19**, 944 (1986).
[35] R. D. Shannon and C. T. Prewitt, Acta Crystallogr. B **25**, 925 (1969).
[36] G. L. Turner, K. A. Smith, R. J. Kirkpatrick, and E. Oldfield, J. Magn. Reson. **70**, 408 (1986).
[37] J. H. Van Vleck, Phys. Rev. **74**, 1168 (1948).
[38] R. M. Sternheimer, Phys. Rev. **84**, 244 (1951).
[39] R. M. Sternheimer, Phys. Rev. **86**, 316 (1952).
[40] R. M. Sternheimer, Phys. Rev. **95**, 736 (1954).
[41] P. W. Langhoff and R. P. Hurst, Phys. Rev. **139**, 1415 (1965).
[42] J. Lahiri and A. Mukherji, Phys. Rev. **141**, 428 (1966).
[43] R. M. Sternheimer, Phys. Rev. **146**, 140 (1966).
[44] E. A. C. Lucken, *Nuclear Quadrupole Coupling Constants* (Academic, London, 1969).